Particle-hole symmetry and interaction effects in the Kane-Mele-Hubbard model

Dong Zheng,[1,2] Guang-Ming Zhang,[1] and Congjun Wu[2]
[1]*State Key Laboratory of Low-Dimensional Quantum Physics and Department of Physics, Tsinghua University, Beijing 100084, China*
[2]*Department of Physics, University of California, San Diego, California 92093, USA*
(Received 1 August 2011; revised manuscript received 31 October 2011; published 15 November 2011)

We prove that the Kane-Mele-Hubbard model with purely imaginary next-nearest-neighbor hoppings has a particle-hole symmetry at half filling. Such a symmetry has interesting consequences including the absence of charge and spin currents along open edges, and the absence of the sign problem in the determinant quantum Monte Carlo simulations. Consequentially, the interplay between band topology and strong correlations can be studied at high numeric precisions. The process that the topological band insulator evolves into the antiferromagnetic Mott insulator as interaction strength increases is studied by calculating both the bulk and edge electronic properties.

DOI: 10.1103/PhysRevB.84.205121 PACS number(s): 05.50.+q, 71.30.+h, 73.43.Nq

I. INTRODUCTION

The precise quantization of the Hall conductance in the integer quantum Hall states is protected by the nontrivial topology of band structures. This topological property is characterized by the Thouless-Kohmoto-Nightingale-den Nijs (TKNN) number, or the Chern number,[1,2] which takes nonzero values only when time-reversal symmetry is broken. In recent years, tremendous progress has been achieved in a new class of topologically nontrivial band insulators in the presence of time-reversal symmetry, which are termed topological insulators.[3–13] Topological insulators exist in both two (2D) and three dimensions (3D) and are characterized by the Z_2 topological index. These topological states have robust gapless helical edge modes with an odd number of channels in 2D[7,14,15] and an odd number of surface Dirac cones in 3D.[11–13] Topological insulators have been experimentally observed in 2D quantum wells through transport measurements[16] and also in 3D systems of Bi_xSb_{1-x}, Bi_2Te_3, Bi_2Se_3, and Sb_2Te_3 through angle-resolved photoemission spectroscopy[17–20] and the absence of backscattering in scanning tunneling spectroscopy.[21–23]

Interaction effects in topological insulators remain an open question. Due to their gapped nature, topological insulators remain stable against weak interactions. However, strong interactions may change their topological properties. For 2D topological insulators, it has been found that two-particle correlated backscattering, which is an interaction effect and is allowed in the time-reversal-invariant Hamiltonian, can gap out the helical edge states by spontaneously developing magnetic ordering under strong repulsive interactions.[14,15] In this case, time-reversal symmetry is spontaneously broken along edges, although the bulk remains paramagnetic. At mean-field level, interaction effects can destabilize the quantum anomalous Hall state of the Haldane-Hubbard model[24] and the 2D topological insulating state of the Kane-Mele-Hubbard (KMH) model[25] by developing long-range charge density wave and antiferromagnetic orders, respectively.[25] Interactions can also change the topologically trivial band structures into nontrivial ones at mean-field level by developing bulk order parameters.[26–29] Due to the difficulty of analytic studies on strong correlation physics, exact results from numeric simulations are desirable. Recently, an exact diagonalization has been carried on the spinless Haldane-Hubbard model.[30] A first-order phase transition between the quantum anomalous Hall insulating state and topologically trivial Mott insulating state is found.

Quantum Monte Carlo (QMC) simulations play an important role in studying strongly correlated systems.[31–34] A major obstacle to applying QMC to fermion systems is the notorious sign problem. In the particular method of the determinant QMC, the 4-fermion interaction terms are decoupled through the Hubbard-Stratonovich (HS) transformation and fermions are able to be integrated out. The resultant fermion determinant, generally speaking, is not positive-definite, which is the origin of the notorious sign problem. This problem prevents QMC simulations from achieving a good numerical precision at low temperatures and large sample sizes. Nevertheless, in a number of interacting models, the sign problem disappears. As presented in Ref. 35, these models include the negative-U Hubbard model, the positive-U Hubbard model at half filling and in bipartite lattices, and a class of models whose interactions can be decomposed in a time-reversal-invariant way.

We find that the Kane-Mele model augmented by the Hubbard interaction with purely imaginary next-nearest-neighbor hoppings has a particle-hole symmetry. Such a symmetry has interesting consequences such as the absence of edge charge and spin currents, which shows the edge currents are not a reliable criterion for topological properties. More importantly, the particle-hole symmetry ensures the absence of the sign problem in the quantum Monte Carlo simulations. This provides a wonderful opportunity to study interaction effects in topological insulating systems. In this article, we perform a determinant QMC study on the stability of the topological insulating state of the KMH model with the strong Hubbard interaction U. Antiferromagnetic long-range order has been found at large values of U. Consequently, the quantum phase diagram of the KMH model can be classified into paramagnetic bulk insulating phases and antiferromagnetic Mott insulating phases. When we further consider the stability of helical edges with infinitesimal two-particle backscattering, which is not contained in the KMH model but is generally allowed by time-reversal symmetry, the paramagnetic bulk insulating phase can be divided into two regimes according to their edge-state Luttinger parameters.[14] The topological band insulator with stable helical edges is stable in the weak interaction regime, while the helical edges become unstable

by two-particle correlated backscattering at the intermediate interaction regime. We have also studied the nature of the spin-liquid phase in the pure Hubbard model with $\lambda = 0$, showing that it is neither a spontaneous Haldane-type quantum anomalous Hall insulator nor a Kane-Mele-type quantum spin Hall insulator. Near the completion of this paper, a similar work on the QMC simulation on the KMH model was performed by Hohenadler *et al.*[36]

This article is organized as follows. In Sec. II, we prove the absence of the sign problem in the KMH model under certain conditions. In Sec. III, we present simulations on the developing of antiferromagnetic long-range orders in the bulk. In Sec. IV, the edge properties are studied including both the edge single-particle excitations and the edge spin correlations. In Sec. V, we present the simulation of the charge and spin current orders in the pure Hubbard model on the honeycomb lattice. Conclusions are given in Sec. VI.

II. GENERAL PROPERTIES OF THE KMH MODEL

The Kane-Mele model is a straightforward generalization of the Haldane model on the honeycomb lattice[7] defined as

$$H_0 = -t \sum_{\langle i,j\rangle,\sigma} c^\dagger_{i\sigma} c_{j\sigma} + i\lambda \sum_{\langle\langle i,i'\rangle\rangle\alpha,\beta} \{c^\dagger_{i\alpha}\sigma_{z,\alpha\beta} c_{i'\beta} - c^\dagger_{i'\alpha}\sigma_{z,\alpha\beta} c_{i\beta}\} - \mu \sum_{i,\sigma} c^\dagger_{i\sigma} c_{i\sigma}, \quad (1)$$

where t is the nearest-neighbor (NN) hopping integral as scaled to 1 below; λ is the next-nearest-neighbor (NNN) spin-orbit hopping integral; μ is the chemical potential. In the general case of the Kane-Mele model, the NNN hoppings for the spin-$\uparrow$ and -$\downarrow$ electrons are complex valued and complex conjugate to each other. As a special case, the NNN hopping in Eq. (1) is purely imaginary. The Hubbard interaction is defined as usual:

$$H_{\rm int} = U \sum_i \left[n_{i\uparrow} - \frac{1}{2}\right]\left[n_{i\downarrow} - \frac{1}{2}\right]. \quad (2)$$

In this section, we will present the symmetry properties of Eqs. (1) and (2), and prove the absence of the sign problem in the determinant QMC.

A. Particle-hole symmetry

Equations (1) and (2) have the particle-hole symmetry at $\mu = 0$ as explained below. We define the transformation as usual:

$$c^\dagger_{i\sigma} \longrightarrow d_{i\sigma} = (-1)^i c^\dagger_{i\sigma}, \quad c_{i\sigma} \longrightarrow d^\dagger_{i\sigma} = (-1)^i c_{i\sigma}. \quad (3)$$

Under this transformation, a Hermitian fermion bilinear operator connecting two sites belonging to two different sublattices transforms as

$$c^\dagger_{i\sigma} K_{ij} c_{j\sigma} + c^\dagger_{j\sigma} (K_{ij})^* c_{i\sigma} \longrightarrow d^\dagger_{i\sigma} (K_{ij})^* d_{j\sigma} + d^\dagger_{j\sigma} K_{ij} d_{i\sigma}, \quad (4)$$

while that connecting two different sites in the same sublattice transforms as

$$c^\dagger_{i\sigma} K_{ii'} c_{i'\sigma} + c^\dagger_{i'\sigma} (K_{ii'})^* c_{i'\sigma} \longrightarrow - d^\dagger_{i\sigma} (K_{ii'})^* d_{i'\sigma} - d^\dagger_{i'\sigma} K_{ii'} d_{i'\sigma}. \quad (5)$$

The on-site particle density transforms as

$$c^\dagger_{i\sigma} c_{i\sigma} - \tfrac{1}{2} \longrightarrow \tfrac{1}{2} - d^\dagger_{i\sigma} d_{i\sigma}, \quad (6)$$

where no summation over spin index is assumed in Eq. (6). Clearly in Eq. (1), the NN hopping is real and the NNN hopping is purely imaginary; thus its band structure is invariant at $\mu = 0$. Equation (2) is obviously invariant. The particle-hole symmetry also implies that $\mu = 0$ corresponds to half filling.

B. Absence of the charge and spin currents

An important conclusion based on the particle-hole symmetry is that both charge and spin currents vanish on all the bonds for the KMH model of Eqs. (1) and (2) at $\mu = 0$. This result applies to arbitrary boundary conditions with broken bonds but with the homogeneous on-site potential which maintains the particle-hole symmetry on each site. The proof is straightforward. Through the continuity equation, the current operators of each spin component along the NN and NNN bonds are defined as

$$J^{\rm NN}_{ij,\sigma} = it(c^\dagger_{i\sigma} c_{j\sigma} - c^\dagger_{j\sigma} c_{i\sigma}), \quad J^{\rm NNN}_{ii',\sigma} = \lambda(c^\dagger_{i\sigma} c_{i'\sigma} + c^\dagger_{i'\sigma} c_{i\sigma}), \quad (7)$$

respectively, where no summation over spin index is assumed. Both $J^{\rm NN}$ and $J^{\rm NNN}$ are odd under the particle-hole transformation; thus they vanish even with the open-boundary condition. By the same reasoning, the charge current also vanishes in the Haldane-Hubbard model with the purely imaginary NNN-hoppings and the particle-hole symmetric charge interactions of

$$H_{\rm NN,int} = \sum_{ij} V_{ij}\left(n_i - \frac{1}{2}\right)\left(n_j - \frac{1}{2}\right). \quad (8)$$

This result shows that edge charge and spin currents are not good criteria for quantum anomalous Hall and topological insulators. In order to have a better understanding of this counterintuitive result, we have considered the simplest noninteracting Haldane model with the purely imaginary NNN hoppings by diagonalization. There are indeed gapless one-dimensional single-particle chiral edge modes clearly seen from the spectra as commonly presented in the literature. Clearly this branch of edge modes contributes to edge currents. However, we find that the continuous bulk spectra also contribute to edge currents. Perfect cancellation occurs which results in zero current on each bond, including each edge bond, although we know for sure that the band structure is topologically nontrivial. For interacting models, there are no well-defined single-particle states. We cannot separate the edge and bulk contributions anymore. Nevertheless, we expect that current correlation functions should exhibit differences between topological insulators and trivial insulators.

Another conclusion inferred from the particle-hole symmetry is that the average particle density for each spin component on each site is strictly $\frac{1}{2}$ even when the translational symmetry is broken. For example, it applies to any disordered pattern of the hopping integrals, as long as the NN hoppings are real and the NNN hoppings are purely imaginary.

Edge currents do appear if the particle-hole symmetry is broken. For example, for the noninteracting Haldane model

with generally complex-valued NNN hoppings, edge currents appear along open boundaries. So far we only consider the sharp edges of broken bonds but with homogeneous on-site potential. For edges with the confining single-particle potential, the particle-hole symmetry is broken which also results in edge currents. In particular, for a weak linear external potential, the linear response should still give rise to quantized Hall conductance in the insulating region.

C. Absence of the QMC sign problem

The Hubbard model on the honeycomb lattice, which corresponds to the case of $\lambda = 0$ of Eqs. (1) and (2), has been recently simulated at half filling.[37] As the Hubbard U increases from zero to a moderate value and then the strong-coupling regime, the ground state emerges from a semimetal phase to a new spin-liquid phase and then to the antiferromagnetic insulating phase. Below we will prove that the sign problem still vanishes with nonzero values of λ.

Just as Ref. 37 does, we employ a discrete HS transformation which respects the SU(2) symmetry for every fixed HS field configuration by decoupling in the density channel. We rewrite the Hubbard interaction and decompose it in the density channel by using imaginary numbers as

$$e^{-\Delta U(n_\uparrow+n_\downarrow-1)^2/2} = \sum_{l=\pm1,\pm2} \gamma_i(l) e^{i\eta_i(l)\sqrt{\Delta\tau\frac{U}{2}}(n_\uparrow+n_\downarrow-1)} + O(\Delta\tau^4), \tag{9}$$

where the discretized HS fields take values of $\gamma(\pm1) = 1+\sqrt{6}/3$, $\gamma(\pm2) = 1-\sqrt{6}/3$; and $\eta(\pm1) = \pm\sqrt{2(3-\sqrt{6})}$, $\eta(\pm2) = \pm\sqrt{2(3+\sqrt{6})}$.

For the convenience of presentation, we prove the absence of the sign problem in the finite-temperature formalism with $\beta = 1/T$. The proof for the zero-temperature projector algorithm is similar. The partition function at half filling reads

$$Z = \sum_{\{l\}} \left\{ \left(\mathrm{Tr} \prod_{p=M}^{1} e^{-\Delta\tau \sum_{i,j} c_{i\uparrow}^\dagger K_{ij}^\uparrow c_{j\uparrow}} e^{i\sqrt{\Delta\tau U/2}\sum_i \eta_{i,p}(l)(c_{i\uparrow}^\dagger c_{i\uparrow}-\frac{1}{2})} \right) \times \left(\mathrm{Tr} \prod_{p=M}^{1} e^{-\Delta\tau \sum_{i,j} c_{i\downarrow}^\dagger K_{ij}^\downarrow c_{j\downarrow}} e^{i\sqrt{\Delta\tau U/2}\sum_i \eta_{i,p}(l)(c_{i\downarrow}^\dagger c_{i\downarrow}-\frac{1}{2})} \right) \times \prod_{i,p} \gamma_{i,p}(l) \right\}, \tag{10}$$

where $\sum_{\{l\}}$ sums over all the configurations of the discrete HS fields $\eta_{i,p}(l)$ and $\gamma_{i,p}(l)$; i and p are indices of discretized grids along the spatial and temporal directions, respectively; Tr takes the trace of the fermion space; $\Delta\tau$ is the discretized time slice which is set to 0.05 in the simulations in this paper; and $M\Delta\tau$ equals the imaginary time β. By using the particle-hole transformation defined in Eq. (3), we show that the on-site particle density transforms according to Eq. (6); the NN-hopping matrix kernel transforms according to Eq. (4); the NNN-hopping matrix kernel transforms according to Eq. (5).

When the following two conditions are satisfied, the fermion determinants of two spin components are complex conjugate to each other; thus the product of them is positive-definite:

$$\begin{aligned} K_{ij}^\sigma &= \left(K_{ji}^{\bar\sigma}\right)^* = K_{ij}^{\bar\sigma} \quad \text{for NN hopping;} \\ K_{ij}^\sigma &= -\left(K_{ji}^{\bar\sigma}\right)^* = -K_{ij}^{\bar\sigma} \quad \text{for NNN hopping.} \end{aligned} \tag{11}$$

Apparently, Eqs. (1) and (2) satisfy these conditions and thus are sign-problem free.

Please note that the KMH mode is sign-problem free only when the NNN hopping is purely imaginary. Generally speaking, the interacting model without the sign problem can have complex-valued hoppings with opposite signs, which still gives rise to opposite Chern numbers for the band structures of spin-↑ and -↓, respectively. However, they are not related by time-reversal symmetry anymore.

III. THE QMC STUDY ON THE BULK PROPERTIES OF THE KMH MODEL

The Hubbard model on the honeycomb lattice, which corresponds the case of $\lambda = 0$ in Eqs. (1) and (2), has been simulated in Ref. 37. When U increases from zero, the single-particle charge gap appears at $U = 3.7$, while the antiferromagnetic long-rang order emerges at $U = 4.3$. The mismatch reveals an exotic spin-liquid phase in between. When the intrinsic spin-orbit coupling, i.e., the NNN hopping term in Eq. (1), enters, the model describes the topological band insulator. It already has a band gap even at $U = 0$. As increasing U, the antiferromagnetic structure factor is still a good quantity to tell when the magnetic long-range order appears. However, the bulk gap is no longer an appropriate quantity to judge a possible transition from the topological band insulator to an antiferromagnetic Mott insulator. Here we use the local single-particle gap on edge sites as an indicator of the stability of edge states and topological properties. We also study the edge effects to antiferromagnetic correlations. In this section, we will simulate the bulk antiferromagnetic structure factor, and leave the study of edge properties to Sec. IV.

A. Sampling parameters of our simulations

Based on the above proof of the absence of the sign problem, we perform the QMC simulation for the KMH model at zero temperature by using the projective method.[38] We perform measurements from 10 different random number series and each independent measurement has 500 sample sweeps after warming up; the discrete imaginary time step $\Delta\tau$ is set to be 0.05. In this section, we use periodic boundary conditions for bulk properties calculation, e.g., the bulk antiferromagnetic structure factor.

B. The developing of the bulk antiferromagnetic long-range order

The spin-orbit NNN hopping in Eq. (1) breaks the SU(2) symmetry but preserves the conservation of S_z. As a result, the antiferromagnetic correlation of S_z should be different from those of S_x and S_y. In the large-U limit, the NNN hopping generates an anisotropic exchange as

$$H_{\mathrm{ex,NNN}} = -J'\left(S_i^x S_{i'}^x + S_i^y S_{i'}^y - S_i^z S_{i'}^z\right) \tag{12}$$

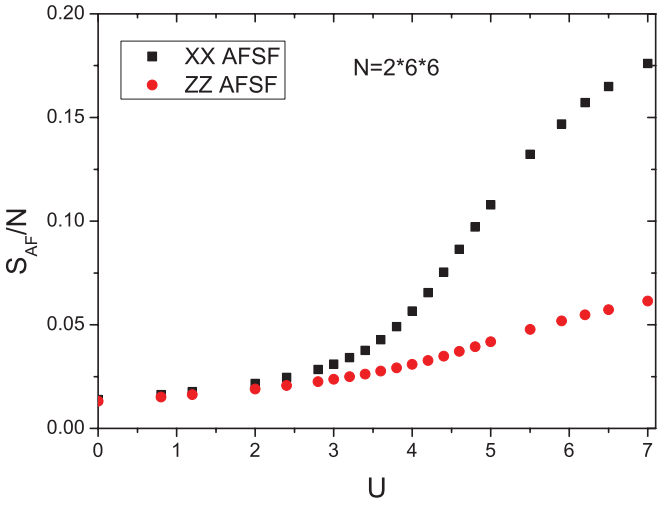

FIG. 1. (Color online) The comparison between the antiferromagnetic structure factors $S^{zz}_{\rm AF}$ along the z axis and $S^{xx}_{\rm AF}$ in the x,y plane at $\lambda = 0.1$ for the size of $N = 2 \times L \times L$ with $L = 6$. The easy-plane feature is clear.

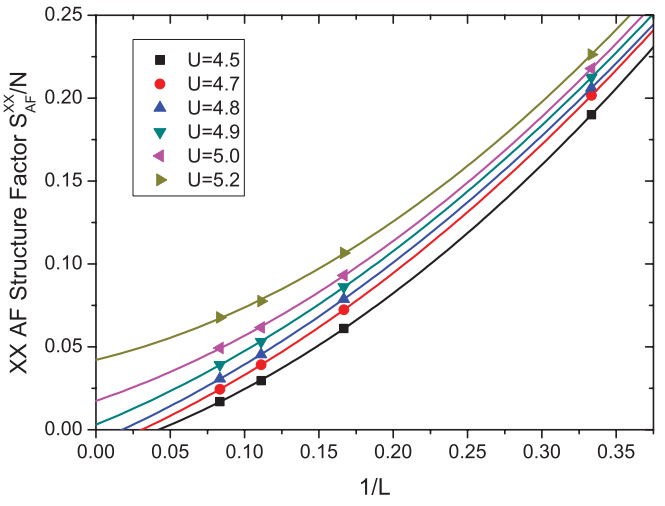

FIG. 2. (Color online) The finite-size scaling of the xx antiferromagnetic structure factors calculated at $\lambda = 0.1$ for the sizes of $N = 2 \times L \times L$ ($L = 3,6,9$, and 12), and the different values of U indicated in the inset. Finite values of $S^{xx}_{\rm AF}/N$ in the thermodynamic limit appear at $U \geqslant U_c$ with $U_c \approx 4.9$.

with $J' = 4\lambda^2/U$, which is ferromagnetic in the x,y plane and antiferromagnetic along the z direction.[25] As the combined effect from the NNN anisotropic exchange and NN isotropic antiferromagnetic exchange, the magnetic exchange along the z axis is frustrated while those along the x and y axes are not. Thus the Néel ordering favors the easy x,y plane.

Our QMC simulations have confirmed this picture. The antiferromagnetic structure factor along the x direction (xx-AFSF) and the z direction (zz-AFSF) are defined as

$$S^{xx}_{\rm AF} = \frac{1}{N}\langle G|\left[\sum_i (-1)^i S^x_i\right]^2|G\rangle,$$
$$S^{zz}_{\rm AF} = \frac{1}{N}\langle G|\left[\sum_i (-1)^i S^z_i\right]^2|G\rangle, \quad (13)$$

where $\langle G|..|G\rangle$ means average over the ground state; $N = 2 \times L \times L$ is the number of sites; L is the size; $(-)^i$ takes the values of ± 1 for the A and B sublattices, respectively. The comparison between $S^{xx}_{\rm AF}$ and $S^{yy}_{\rm AF}$ is plotted in Fig. 1, which clearly shows the easy-plane feature.

Below we will use the xx-AFSF to describe the antiferromagnetic properties and perform the simulation at $\lambda = 0.1$ with different values of U and sample sizes of $L = 3,6,9,12$. The extrapolation to the thermodynamic limit for different Hubbard U is plotted in Fig. 2. It can be seen that the magnetic long-range order emerges at $U_c = 4.9 \pm 0.1$ for $\lambda = 0.1$. In Fig. 3 we present the QMC simulation on the magnetic phase diagram of the KMH model in the parameter space of (U,λ). The phase boundary separating the AF long-range-ordered phase and nonmagnetic phases is marked for various values of λ. The spin-orbit coupling opens the band gap at the order of λ; thus the interaction effect U becomes important only when U is larger than λ. As a result, the critical value of U_c for the onset of the AF phase increases with λ.

The phase diagram Fig. 3 exhibits a large regime of nonmagnetic insulating state outside the AF phase at $\lambda \neq 0$. At small values of U, it should be the Z_2 topological band insulator which is stable against weak interactions. As increasing U, it enters the AF Mott insulating phase at a critical line of U_c. In an updated version of Ref. 36, it is found that the spin-liquid phase also extends to a small but finite value of λ. However, the nature of this spin-liquid state remains unclear. The bulk paramagnetic regime actually has rich internal structures. According to the stability of the helical edge states with respect to the two-particle spin-flip backscattering, this paramagnetic insulating phase is divided into two different regimes with the effective edge Luttinger parameter $K < (>)\frac{1}{2}$, respectively. The analysis is presented below in Sec. IV C.

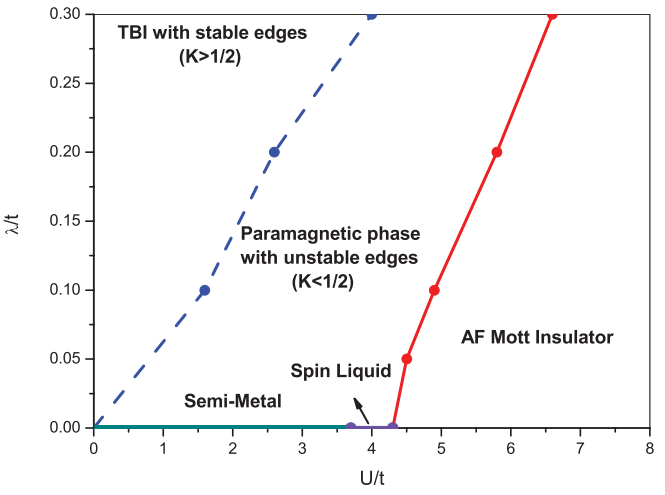

FIG. 3. (Color online) The QMC simulation of the phase diagram of the KMH model. The antiferromagnetically long-range-ordered phase appears at strong correlation regime. The paramagnetic phase is divided into two regimes: topological band insulator (TBI) with stable helical edges, and bulk paramagnetic phase with unstable edges (see further discussions in Sec. IV C). The two critical values of U at $\lambda = 0$ are from Ref. 37 by Meng *et al.*, which are also confirmed in our QMC simulations.

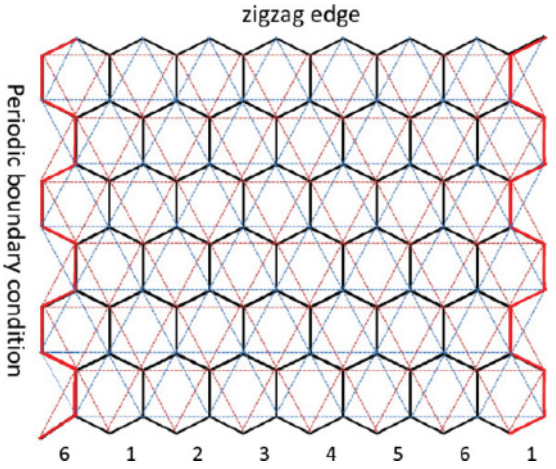

FIG. 4. (Color online) The KMH model in the lattice with the zigzag edges. The boundary conditions are periodical and open along the x and y directions, respectively. The NNN bonds between two closest tips on the zigzag edges are removed.

IV. THE QMC STUDY OF THE EDGE PROPERTIES OF THE KMH MODEL

We believe that the edge properties are crucial to expose the topological aspect of the KMH model. In this section, we will show that the antiferromagnetic correlations along the edge becomes strongly relevant as the Hubbard U increases while the bulk remains paramagnetic. We consider the lattice configuration plotted in Fig. 4 with the periodical and open boundary conditions along the x and y directions, respectively.

A. The single-particle excitations

As proved in Sec. II, the edge currents, both for charge and spin, are always zero due to the particle-hole symmetry. We use another quantity, the local single-particle excitation gap on edge sites, to check whether the edges are gapped or gapless. It can be extracted from the tail of the on-site time-displaced Green's function on the edge $\ln G(i,i;\tau) \sim \Delta_{\text{edge}}\tau$, which is defined by

$$G(i,i;\tau) = \frac{1}{L}\langle G| \sum_{i\in \text{tip}} c^{\dagger}_{i\uparrow}(\tau)c_{i\uparrow}(0) + c^{\dagger}_{i\downarrow}(\tau)c_{i\downarrow}(0)|G\rangle, \quad (14)$$

where $|G\rangle$ is the many-body ground state. The dependency of $\ln G(i,i;\tau)$ with τ for the site i on the tip of the zigzag edges is plotted in the inset of Fig. 5, where the long tail of $\ln G(i,i;\tau)$ shows a linear behavior with τ and the slope measures the excitation gap. Here the lattice has a ribbon geometry with n_y zigzag rows. We fix the width of the ribbon $n_y = 8$ and increase its length. The extrapolations of the edge excitation gaps with L are depicted in Fig. 5 with λ fixed at 0.1 and different values of $U < U_c$. Clearly increasing U significantly reduces the weight of the low-energy spectra.

The bosonization analysis of the stability of the helical edge states has been performed in Refs. 14 and 15. For the parameter regime of Fig. 5, the bulk remains paramagnetic, or, time-reversal invariant. For the current KMH model, S_z is conserved which prohibits the existence of the two-particle

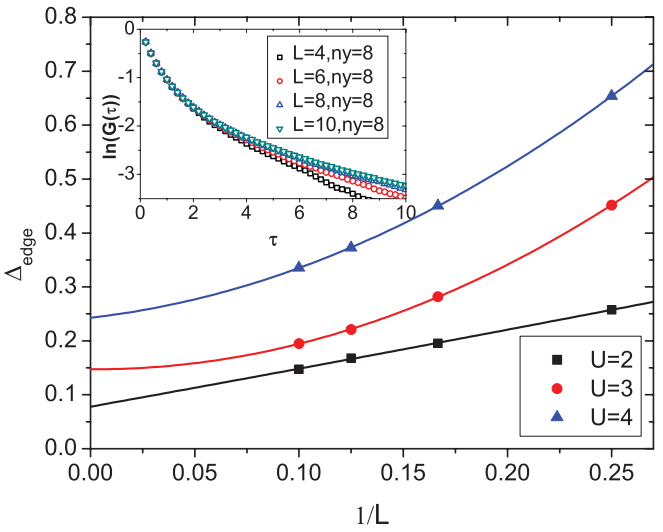

FIG. 5. (Color online) The extrapolation of local single particle gap for the tip sites on the zigzag edges of a ribbon geometry with the size of $2 \times L \times n_y$ with $n_y = 8$. In the inset, the logarithms of on-site time-displaced Green's functions $\ln G(i,i;\tau)$ of the tip sites is depicted for $U = 2$. The slopes of the long time tails measure the edge excitation gap Δ_{edge}. Here λ is set to be 0.1 in this calculation. We want to emphasize that the finite gap in the bulk paramagnetic phase is a limitation of system size, as the edge should be gapless due to $U(1)$ symmetry.

spin-flip scattering term to open the gap. The Luttinger-liquid theory of such a helical edge branch, i.e., the right and left movers are with opposite spin polarizations, is characterized by only one Luttinger parameter K, which describes the forward scattering between these two branches. Due to the helical nature of the edge states, the long-wavelength charge fluctuations and the z component of the spin fluctuations are not independent but are conjugate to each other. Both of them are gapless in the thermodynamic limit, and so are the single-particle edge excitations. The on-site imaginary time single-particle Green's function decays as $1/\tau^{\alpha}$ with the exponent

$$\alpha = K + 1/K. \quad (15)$$

At $K \ll 1$, the low-energy density of states does not open a full gap but is depleted according to a power law, and thus exhibits a pseudogap behavior. The nonzero gap values in Fig. 5 may be an artifact of finite-size scaling and a result of tunneling between two opposite edges. A more detailed numerical analysis is needed to further clarify the nature of the single-particle excitations.

B. Edge spin structure factors

We further investigate the edge effects to the antiferromagnetic correlations. We define the antiferromagnetic structure form factor for each zigzag row parallel to the zigzag boundary as

$$S^{xx}_{\text{Zigzag,AF}}(m) = \frac{1}{2L}\langle G|\left[\sum_i (-1)^i S^x_{m,i}\right]^2 |G\rangle, \quad (16)$$

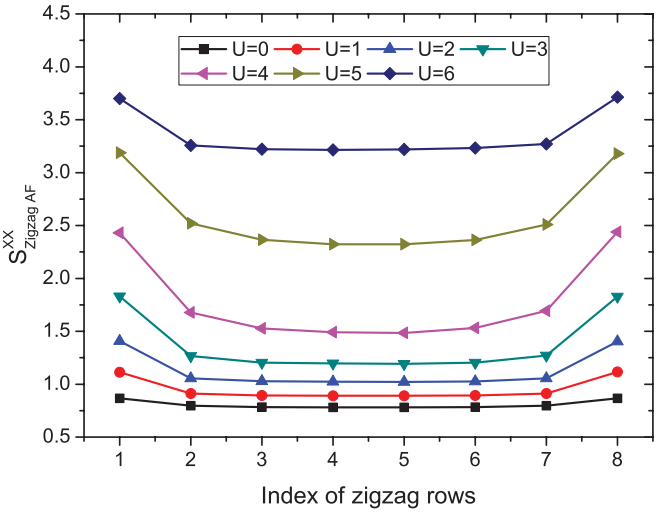

FIG. 6. (Color online) The row xx-AFSF defined in Eq. (16) for each zigzag rows parallel to the boundary. The parameters values are $\lambda = 0.1$; the sample size $2 \times L \times L$ with $L = 8$; and the different values of U are indicated in the inset. The row indices 1 and 8 correspond to the boundary rows, and those of 4 and 5 corresponds to the central rows.

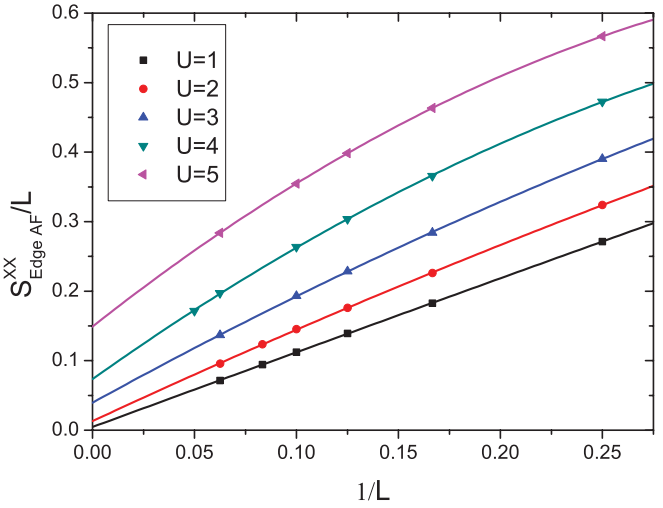

FIG. 7. (Color online) The finite-size scaling of the xx-AFSF defined in Eq. (16) for the edge row with $\lambda = 0.1$. The size of this ribbon is $2 \times L \times 4$. We emphasize that due to the 1D nature of the edge and the $U(1)$ spin symmetry, this scaling actually shows the power-law correlation rather than the true long-range order. The finite intercepts are mainly due to small-size effects.

where m is the index of the zigzag row, i is the site index along the mth zigzag line, and $2L$ is the number of sites in each row. The xx-AFSF for all the rows are depicted in Fig. 6.

It is interesting to observe that the AF correlations are strongest on the edges and become weaker inside the bulk. This effect is most prominent at small and intermediate values of U, because the single-particle band gap due to λ is suppressed around the edges, which enhances the interaction effects. When $U \geqslant U_c \approx 4.9$, the bulk antiferromagnetism develops. The antiferromagnetic correlations along both the edge and central rows are enhanced by U. However, their difference is suppressed due to the disappearance of the helical edge states.

The finite-size scaling of the xx-AFSF for the edge rows for different values of U is presented in Fig. 7. Compared with the xx-AFSF calculated in the bulk (Fig. 2), the edge antiferromagnetic correlations are much stronger than those of the bulk. Although the extrapolation to the infinite size in Fig. 7 implies a finite value of the Néel order of S_x on the edge, we believe that it is an artifact due to the power-law scaling of the AF correlations. The 1D nature of the edge states and the conservation of S_z prohibits the true long-range Néel ordering of $S_{x,y}$ but allows the quasi-long-range ordering, which is confirmed in the two-point spin correlations in Sec. IV C.

C. The stability of the helical edges

According to the bosonization analysis in Ref. 14, the scaling dimension of the $2k_f$ Néel order of the x, y components is K; thus their equal-time correlations decay as $1/|x - x'|^{2K}$. If the condition of the conservation of S_z is released, a time-reversal-invariant two-particle correlated spin-flip backscattering term is allowed as

$$H_{bg,2pct} = \int dx \psi^\dagger_{R\uparrow} \partial_x \psi^\dagger_{R\uparrow} \psi_{L\downarrow} \partial_x \psi_{L\downarrow} + \text{H.c.} \qquad (17)$$

At the particle-hole symmetric point of the KMH model that we are simulating, the above term becomes the Umklapp term which conserves the lattice momentum. Such a term reduces the $U(1)$ spin symmetry down to Z_2. It has the scaling dimension $4K$ and becomes relevant at $K < K_c = 1/2$. In this case, it opens a gap by developing the long-range $2k_f$ magnetic ordering of S_x or S_y. Even for the cases that the two-particle spin-flip backscattering are random disordered or at a single site, they still can destabilize the helical edge states at smaller values of the Luttinger parameter K.[14]

According to the above analysis, the bulk paramagnetic regime at weak and intermediate coupling strengths should be divided into two regimes. At weak interactions, the helical edge states are stable against interaction effects. The two-particle backscattering terms only have perturbative effects. On the other hand, at intermediate levels of interaction strength, interaction effects are nonperturbative which breaks time-reversal symmetry along edges and thus destroys the helical edges. We emphasize that this destabilizing of helical edges occurs when the bulk remains paramagnetic and time-reversal invariant.

To numerically verify this picture, we present the calculation of the real-space equal-time two-point correlations along the zigzag edge in Fig. 8. Since each unit cell contains two nonequivalent sites, we denote the sites on the tips of the edge as A sites and the other slightly inner sites as B sites. The correlation functions are defined as

$$\begin{aligned} C_{AA}(r,r') &= \langle G|S^A_x(\vec{r})S^A_x(\vec{r}')|G\rangle, \\ C_{BB}(r,r') &= \langle G|S^B_x(\vec{r})S^B_x(\vec{r}')|G\rangle, \\ C_{AB}(r,r') &= \tfrac{1}{2}\{\langle G|S^A_x(\vec{r})S^B_x(\vec{r}')|G\rangle \\ &\quad + \langle G|S^B_x(\vec{r})S^A_x(\vec{r}')|G\rangle\}, \end{aligned} \qquad (18)$$

where $\vec{r}$ and $\vec{r}'$ are along the zigzag edge. The simulated results for $\lambda = 0.1$ are plotted at different values of U in

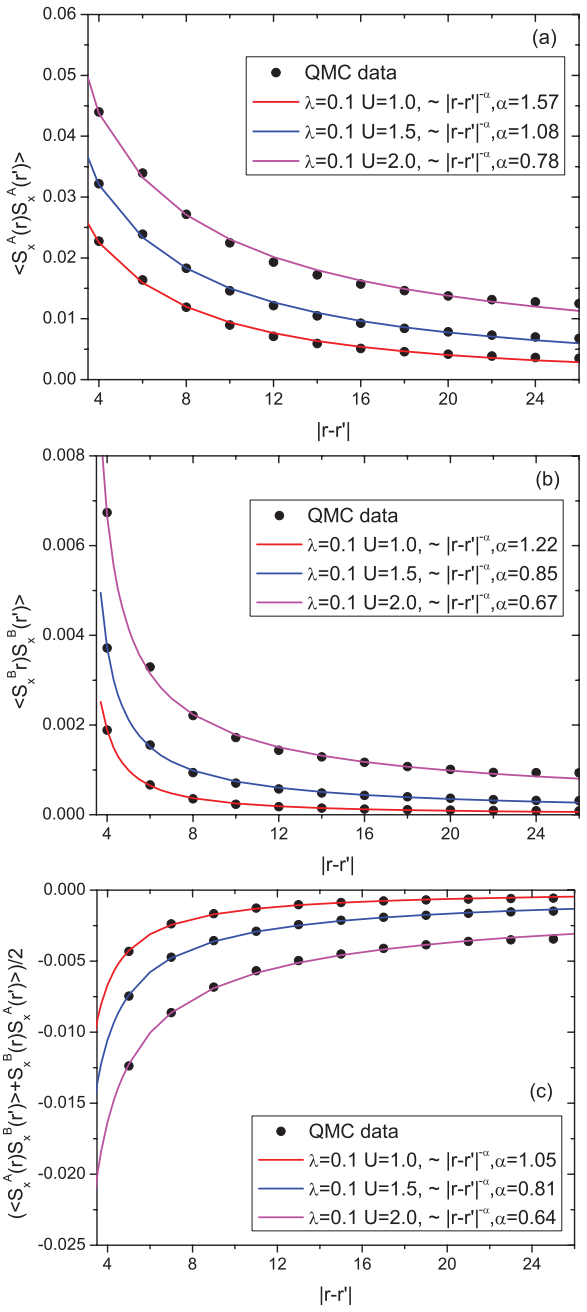

FIG. 8. (Color online) The two-point equal-time spin correlation functions along the zigzag edge with $\lambda = 0.1$ at values of U denoted in the insets. The size of the ribbon is $2 \times 34 \times 4$. Because the zigzag edge contains the sites of both A and B type, three different types of correlations are plotted in (a), (b), and (c), respectively. The Luttinger parameters are fitted from the correlation among A sites on the tips as $K \approx 0.8, 0.5$, and 0.4 for $U = 1, 1.5$, and 2, respectively.

the bulk paramagnetic regime. The edge-spin correlation exhibits the ferrimagnetic correlations among A and B sites because the edge breaks the equivalence between A and B sites. The magnetic correlations are stronger among the outer A sites, and are weaker among the inner B sites. All of these correlations obey the power law and their decay exponents (α) are fitted. As U increases further toward to the bulk antiferromagnetic regime, the difference between AA and BB correlations becomes weaker.

Due to the domination of the magnetic correlation at A sites, we use the decay exponents of C_{AA} to fit the effective Luttinger parameter K for the helical edge. The three plots in Fig. 8(a) at $U = 1, 1.5$, and 2 give rise to $K = \frac{1}{2}\alpha \approx 0.8, 0.5$, and 0.4, respectively. The case of $U = 1$ belongs to the topological band insulating phase in which interaction effects are perturbative. For the case of $U = 2$ at which the bulk remains nonmagnetic, although the edge remains gapless, this is only because of the conservation of S_z which is *not* an essential symmetry of topological insulators. As long as the above Umklapp term Eq. (17) is introduced, which unfortunately cannot be simulated by our QMC method, the gapless helical edge states are destabilized. We argue that the system enters a new phase with paramagnetic bulk but unstable edges. The transition point between these two paramagnetic phases at $\lambda = 0.1$ lies at $U \approx 1.5$ with $K \approx 0.5$.

We have calculated the edge-spin correlations for other values of spin-orbit coupling and interaction parameters to map the boundary with $K = 0.5$ between two different bulk paramagnetic phases. The boundary is plotted in Fig. 3. As λ decreases, the dispersion of the edge spectra becomes more flat and interaction effects become stronger. As a result, the boundary shifts to lower values of U. In particular at $\lambda = 0$, the edge spectra become exactly flat; we expect edge ferromagnetism at infinitesimal U due to the density of state divergence. Thus the boundary should pass the origin. In particular, the edge ferromagnetism of the graphene ribbon has been simulated.

V. ABSENCE OF SPIN-ORBIT ORDER IN SPIN-LIQUID PHASE AT $\lambda = 0$

Since Meng *et al.*[37] claimed the existence of a spin-liquid phase for the Hubbard model ($\lambda/t = 0$) at $3.7 < U/t < 4.3$ (see Fig. 3), there has been considerable interest and debate on the nature of this phase. One possibility of such a phase is that it could be a relative spin-orbit symmetry-breaking phase with

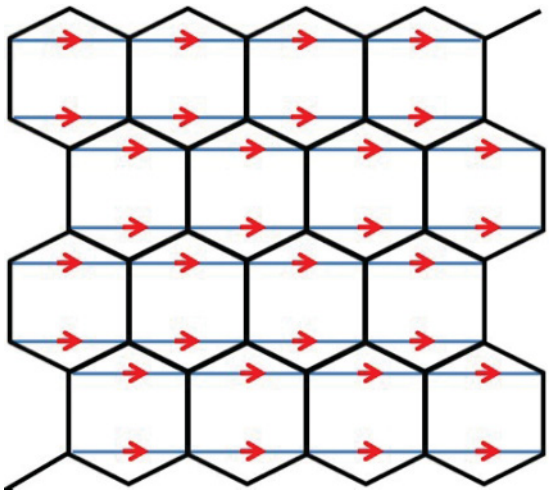

FIG. 9. (Color online) The definition of the positive direction for the NNN bonds on the honeycomb lattice, based on which the NNN current form factors Q_C^{AF} and Q_S^{AF} are defined in Eq. (19).

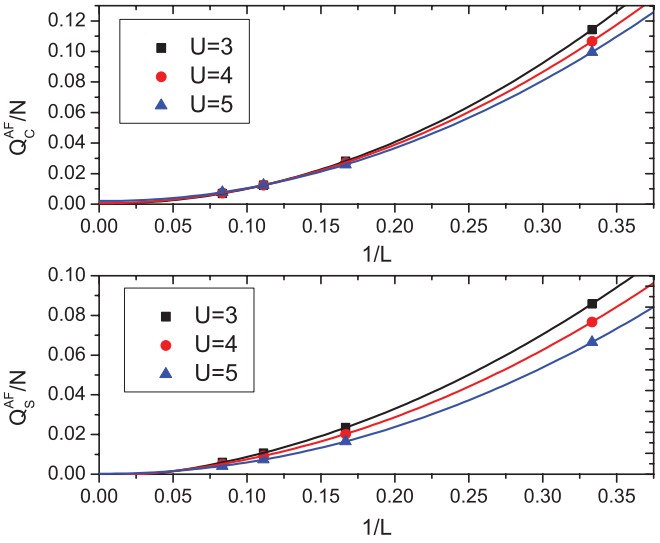

FIG. 10. (Color online) The finite-size scaling of the form factors of the NNN currents in the charge sector Q_c^{AF} and Q_S^{AF} in the spin sector as defined in Eq. (19). The periodical boundary condition is employed. The sample size is $N = 2 \times L \times L$ with $L = 3,6,9$, and 12. λ is set 0 in this calculation, and $U = 3$, 4, and 5.

a nontrivial mean-field band structure.[39] If this is the case, a finite λ/t behaves like an external field to pin down the order parameter along the external spin-orbit configuration. Then the semimetal and spin-liquid phase are indistinguishable at finite λ/t. In this section, we will check the form factor of such a spin-orbit order parameter between NNN sites at $\lambda = 0$, and find negative results.

Without loss of generality, we only consider the horizontal bonds. We define the positive directions for the NNN horizontal bonds as depicted in Fig. 9. Two different NNN current orders are designed, including the charge flux order and the Kane-Mele-type spin-orbit order, or, equivalently, the spin-current flux order. Their form factors are denoted as Q_C^{AF} and Q_S^{AF} and are defined as

$$Q_C^{\mathrm{AF}} = \frac{1}{N}\langle G|\left\{\sum_i (-1)^i J^C_{i,i+\vec{e}_x}\right\}^2|G\rangle,$$
$$Q_S^{\mathrm{AF}} = \frac{1}{N}\langle G|\left\{\sum_i (-1)^i J^S_{i,i+\vec{e}_x}\right\}^2|G\rangle, \tag{19}$$

where $(-)^i$ takes the values of 1 or -1 for site i in the A and B sublattices, respectively; the charge current $J^C_{i,i+\vec{e}_x} = J^{\mathrm{NNN}}_{i,i+\vec{e}_x;\uparrow} + J^{\mathrm{NNN}}_{i,i+\vec{e}_x;\downarrow}$, and spin current $J^S_{i,i+\vec{e}_x} = J^{\mathrm{NNN}}_{i,i+\vec{e}_x;\uparrow} - J^{\mathrm{NNN}}_{i,i+\vec{e}_x;\downarrow}$; $\vec{e}_x$ is the NNN vector along the horizontal direction. Please note that the bond current operator here $J^{\mathrm{NNN}}_{i,i+\vec{e}_x;\sigma}$ is different from that in Eq. (7) as

$$J^{\mathrm{NNN}}_{i,i+\vec{e}_x;\sigma} = i\{c^\dagger_{i,\sigma}c_{i+\vec{e}_x,\sigma} - \mathrm{H.c.}\}, \tag{20}$$

where no summation over σ is assumed.

We have performed the simulation of the NNN charge and spin-current form factors defined in Eq. (19) for the Hubbard model at $\lambda = 0$. The extrapolations of the form factors to the infinite lattice size are depicted in Fig. 10. The curves represent three typical Hubbard U values $U = 3$,4, and 5, which fall in the semimetal phase, spin-liquid phase, and Mott insulating phase, respectively. For all three parameters, both the charge and spin NNN current antiferromagnetic form factors vanish in the thermodynamic limit, indicating the absence of the NNN charge and spin-current orders in all these three phases, especially the spin-liquid phase. The nature of this spin-liquid phase, whether it is actually a subtly ordered phase or a genuinely exotic phase with nontrivial topological properties, remains an unsolved question.

VI. CONCLUSIONS

We have studied the particle-hole symmetry in the KMH model, which results in the absence of the charge and spin currents and the absence of the quantum Monte Carlo sign problem. The determinant QMC simulations have been performed for both the bulk and edge properties. The bulk antiferromagnetic long-range order appears at large values of U. With the open boundary condition, the antiferromagnetic correlation is strongest along the edges. We also discussed the stability of helical edges in the paramagnetic insulating phase when turning on the infinitesimal two-particle backscattering term, which can be introduced by time-reversal-invariant but nonconservation-of-S_z interaction terms, e.g., Rashba terms. The paramagnetic insulating phase in Fig. 3 can be classified into two regimes of weak and intermediate interactions, respectively. In the weak-interaction regime, the helical edge states remain gapless which is robust against the two-particle backscattering; in the intermediate-interaction regime, the edge states can spontaneously break time-reversal symmetry by developing magnetic ordering along the edge by the two-particle backscattering term. Since this destabilizing helical edge occurs when the bulk remains time-reversal invariant, it is an interesting and open question whether the nontrivial bulk Z_2 topology is still maintained in this regime.

We also checked that the spin-liquid phase in the Hubbard model at $\lambda = 0$ on the honeycomb lattice is neither a spontaneously developed Haldane-type quantum anomalous Hall insulator nor the Kane-Mele-type quantum spin Hall insulator.

ACKNOWLEDGMENTS

C.W. and D.Z. thank J. E. Hirsch for his education on the determinate quantum Monte Carlo simulations and his encouragement on this work. C.W. is grateful to S. Kivelson for suggesting the simulation in Sec. V and thanks L. Balents, L. Fu, and T. Xiang for helpful discussions. C.W. is supported by ARO-W911NF0810291 and the Sloan Research Foundation. D.Z and G.M.Z. are supported by the NSF of China and the National Program for Basic Research of MOST-China.

[1]D. J. Thouless, M. Kohmoto, M. P. Nightingale, and M. den Nijs, Phys. Rev. Lett. **49**, 405 (1982).
[2]M. Kohmoto, Ann. Phys. **160**, 296 (1985).
[3]X. Qi and S. Zhang, e-print arXiv:1008.2026.
[4]M. Z. Hasan and C. L. Kane, Rev. Mod. Phys. **82**, 3045 (2010).

[5]B. A. Bernevig, T. L. Hughes, and S.-C. Zhang, Science **314**, 1757 (2006).
[6]X.-L. Qi, T. L. Hughes, and S.-C. Zhang, Phys. Rev. B **78**, 195424 (2008).
[7]C. L. Kane and E. J. Mele, Phys. Rev. Lett. **95**, 146802 (2005).
[8]D. N. Sheng, Z. Y. Weng, L. Sheng, and F. D. M. Haldane, Phys. Rev. Lett. **97**, 036808 (2006).
[9]J. E. Moore and L. Balents, Phys. Rev. B **75**, 121306 (2007).
[10]R. Roy, Phys. Rev. B **79**, 195321 (2009).
[11]L. Fu, C. L. Kane, and E. J. Mele, Phys. Rev. Lett. **98**, 106803 (2007).
[12]L. Fu and C. L. Kane, Phys. Rev. B **76**, 045302 (2007).
[13]H. Zhang, C.-X. Liu, X.-L. Qi, X. Dai, Z. Fang, and S.-C. Zhang, Nature Phys. **5**, 438 (2009).
[14]C. Wu, B. A. Bernevig, and S.-C. Zhang, Phys. Rev. Lett. **96**, 106401 (2006).
[15]C. Xu and J. E. Moore, Phys. Rev. B **73**, 045322 (2006).
[16]M. König, S. Wiedmann, C. Brüne, A. Roth, H. Buhmann, L. W. Molenkamp, X. L. Qi, and S. C. Zhang, Science **318**, 766 (2007).
[17]D. Hsieh, D. Qian, L. Wray, Y. Xia, Y. S. Hor, R. J. Cava, and M. Z. Hasan, Nature (London) **452**, 970 (2008).
[18]D. Hsieh, Y. Xia, L. Wray, D. Qian, A. Pal, J. H. Dil, J. Osterwalder, F. Meier, G. Bihlmayer, C. L. Kane, Y. S. Hor, R. J. Cava, and M. Z. Hasan, Science **323**, 919 (2009).
[19]Y. Xia, D. Qian, D. Hsieh, L. Wray, A. Pal, H. Lin, A. Bansil, D. Grauer, Y. S. Hor, R. J. Cava, and M. Z. Hasan, Nature Phys. **5**, 398 (2009).
[20]Y. L. Chen, J. G. Analytis, J.-H. Chu, Z. K. Liu, S.-K. Mo, X. L. Qi, H. J. Zhang, D. H. Lu, X. Dai, Z. Fang, S. C. Zhang, I. R. Fisher, Z. Hussain, and Z.-X. Shen, Science **325**, 178 (2009).
[21]P. Roushan, J. Seo, C. V. Parker, Y. S. Hor, D. Hsieh, D. Qian, A. Richardella, M. Z. Hasan, R. J. Cava, and A. Yazdani, Nature (London) **460**, 1106 (2009).
[22]Z. Alpichshev, J. G. Analytis, J.-H. Chu, I. R. Fisher, Y. L. Chen, Z. X. Shen, A. Fang, and A. Kapitulnik, Phys. Rev. Lett. **104**, 016401 (2010).
[23]T. Zhang, P. Cheng, X. Chen, J.-F. Jia, X. Ma, K. He, L. Wang, H. Zhang, X. Dai, Z. Fang, X. Xie, and Q.-K. Xue, Phys. Rev. Lett. **103**, 266803 (2009).
[24]Z. Cai, S. Chen, S. Kou, and Y. Wang, Phys. Rev. B **78**, 035123 (2008).
[25]S. Rachel and K. Le Hur, Phys. Rev. B **82**, 075106 (2010).
[26]S. Raghu, X.-L. Qi, C. Honerkamp, and S.-C. Zhang, Phys. Rev. Lett. **100**, 156401 (2008).
[27]K. Sun, H. Yao, E. Fradkin, and S. A. Kivelson, Phys. Rev. Lett. **103**, 046811 (2009).
[28]Y. Zhang, Y. Ran, and A. Vishwanath, Phys. Rev. B **79**, 245331 (2009).
[29]J. Wen, A. Ruegg, C. C. Joseph Wang, and G. A. Fiete, Phys. Rev. B **82**, 075125 (2010).
[30]C. N. Varney, K. Sun, M. Rigol, and V. Galitski, Phys. Rev. B **82**, 115125 (2010).
[31]R. Blankenbecler, D. J. Scalapino, and R. L. Sugar, Phys. Rev. D **24**, 2278 (1981).
[32]J. E. Hirsch, Phys. Rev. B **31**, 4403 (1985).
[33]S. Chandrasekharan and U.-J. Wiese, Phys. Rev. Lett. **83**, 3116 (1999).
[34]S. E. Koonin, D. J. Dean, and K. Langanke, Phys. Rep. **278**, 1 (1997).
[35]C. Wu and S.-C. Zhang, Phys. Rev. B **71**, 155115 (2005).
[36]M. Hohenadler, T. C. Lang, and F. F. Assaad, Phys. Rev. Lett. **106**, 100403 (2011).
[37]Z. Y. Meng, T. C. Lang, S. Wessel, F. F. Assaad, and A. Muramatsu, Nature (London) **464**, 847 (2010).
[38]F. F. Assaad and H. G. Evertz, in Computational Many-Particle Physics, Lecture Notes in Physics 739, edited by H. Fehske, R. Schneider, and A. Weiße (Springer, Berlin, 2008), p. 277.
[39]S. Kivelson (private communication).